HgCdTe e-APD detector arrays with single photon sensitivity for space lidar applications

Xiaoli Sun*[a], James B. Abshire[a], Jeffrey D. Beck[b]
[a]NASA Goddard Space Flight Center, Code 694/690, Greenbelt, MD USA 20771;
[b]DRS C4ISR Group, Dallas, TX USA 75374
*Xiaoli.sun-1@nasa.gov

ABSTRACT

A multi-element HgCdTe electron initiated avalanche photodiode (e-APD) array has been developed for space lidar applications. The detector array was fabricated with 4.3-μm cutoff HgCdTe which covered a spectral response from 0.4 to 4.3 μm. We have characterized a 4x4 detector array with 80 μm square elements and an integrated custom cryogenic silicon read-out integrated circuit (ROIC). The device operated at 77K inside a small closed-cycle Dewar. Measurements showed a unity gain quantum efficiency of about 90% at 1.55 μm. The bulk dark current of the HgCdTe e-APD at 77K was less than 50,000 input referred electrons/s at 12 V APD bias where the APD gain was 620 and the measured noise equivalent power (NEP) was 0.4 fW/Hz$^{1/2}$. The electrical bandwidth of the ROIC was about 6 MHz, which was chosen to match the laser pulse width of our CO_2 lidar. Even with the relatively low bandwidth, the high APD gain and low dark current enabled the device to detect single photon events. Because the APD was biased below the break-down voltage, the detector output was linear with the input optical signal and there was no dead-time and afterpulsing. A new series of HgCdTe e-APDs are being developed with a much wider bandwidth ROIC and higher gain HgCdTe e-APD array, which is expected to give a much better performance in linear mode photon counting applications.

Keywords: HgCdTe, APD, single photon detector, lidar.

1. INTRODUCTION

NASA is developing several Integrated Path Differential Absorption (IPDA) lidar approaches as candidates for its planned Active Sensing of CO_2 Emission over Days, Nights and Seasons (ASCENDS) Mission. The mission's goals are to accurately measure the global distribution of CO_2 in the atmosphere, enabling more accurate estimates of CO_2 sources and sinks.[1] Other programs at NASA are developing similar lidar to measure the column abundance of other greenhouse gasses, such as methane, from orbit.[2] To match favorable absorption bands of atmospheric gases and minimize solar background light, these lidar use near infrared lasers that emit in the wavelength range between 1.5 to 3.2 μm.

To date there has been a lack of high performance photodetectors that are sensitive in this wavelength range. Silicon avalanche photodiodes (APD) have a sharp cutoff near 1 μm. InGaAs APDs are often used for the short wave infrared (SWIR) wavelength to about 1.7 μm, but they have low gain and high excess noise factor when operated in linear mode. InGaAs single photon avalanche photodiodes (SPAD), in which the APD is biased above the break-down voltage, have a relative long recovery time upon each photon detection or a noise event. They also have significant afterpulsing after each avalanche break-down, especially when the SPAD is cooled to maintain an acceptable dark count rate. As a result InGaAs SPAD have to be gated to allow the afterpulsing to dissipate. These nonlinear effects severely limit the applications of InGaAs SPADs in lidar where the signal dynamic range spans 2 to 3 orders of magnitude and the signal arrival time is difficult to predict. Photomultiplier tubes with InGaAs photocathodes can be operated in linear mode to detect single photons for wavelengths up to 1.6 μm but the photon detection efficiency is only a few percent and the dynamic range is usually too narrow for an orbiting lidar.

One of the new and promising detector technologies is the HgCdTe electron initiated avalanche photodiode (e-APD) recently developed by DRS Technologies.[3,4] These detectors operate in linear mode with a near 90% quantum efficiency from 0.4 to 4.3 μm, high APD gain, and an integrated low noise read-out integrated circuit (ROIC). Recent progress in miniaturized space cryogenic cooler[5] has made it practical to use these HgCdTe e-APDs for IPDA lidar, including the CO_2 lidar on the ASCENDS mission.

Advanced Photon Counting Techniques VIII, edited by Mark A. Itzler, Joe C. Campbell, Proc. of SPIE
Vol. 9114, 91140K · © 2014 SPIE · CCC code: 0277-786X/14/$18 · doi: 10.1117/12.2053757

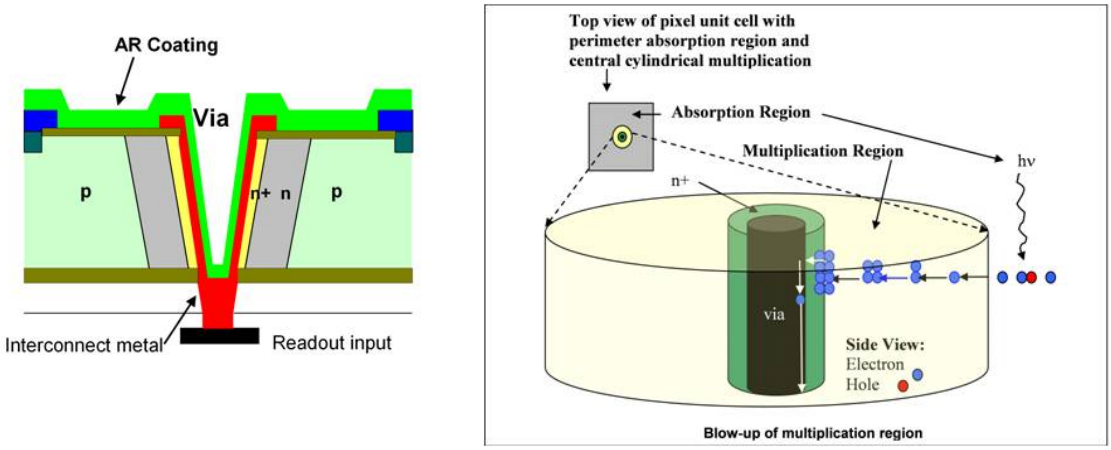

Figure 1. Schematic diagram of the HDVIP structure HgCdTe e-APD by DRS Technologies.

The HgCdTe e-APD design is based on the highly successful High Density Vertically Integrated Photodiode (HDVIP®) architecture developed by DRS Technologies. The HDVIP device is a front-side illuminated, cylindrical, p-around-n photodiode that is formed around a small via in the HgCdTe, as shown in Figure 1. The via also serves as the interconnect conduit between the n-side of the photodiode and the input to the ROIC. Electron and hole pairs excited by incoming photons in the p-region undergo photo-electron multiplications with electrons traveling through the p-n junction to initiate the avalanche process. The APD gain for this type of devices is much less random compared to silicon APDs because of extremely low hole to electron ionization coefficient ratio and the multiplication region that is typically shorter than the mean free path between scattering events. The HDVIP structure is currently employed in mid-wave infrared (MWIR) and low-wave infrared (LWIR) staring arrays in production at DRS. They have several major advantages: (1) interdiffused CdTe passivation of both surfaces; (2) thermal cycle reliability that is array size independent; (3) low defects due to diode junction orientation with respect to threading dislocations; and (4) front side illumination for high quantum efficiency from the visible to the infrared cutoff wavelength determined by the material. For a 4.3 µm cutoff wavelength device the typical APD gain at 77K is greater than 500 and the bulk dark current is less than 50,000 electrons per second per pixel at 12 volts APD bias. DRS has a mature technology to integrate the HgCdTe e-APD with custom low noise cryogenic ROIC to achieve near quantum limited detector performance.

DRS designed and fabricated a set of 4x4 pixel HgCdTe e-APD arrays for the CO_2 lidar[6] supported by NASA's Earth Science Technology Office (ESTO) Instrument Incubator Program (IIP). The pixel pitch was 80 µm. The ROIC was modified to have 16 independent channels in parallel. ROIC electrical bandwidth was chosen to match the 50-ns rise and fall times of the CO_2 lidar's transmitted pulse. The ROIC design was modified from earlier generation devices to further reduce the noise and improve the linear dynamic range. The HgCdTe e-APD arrays were attached to a silicon substrate, which also served as a fan-out of electrical connections for each pixel. The ROIC was placed on the substrate next to the HgCdTe e-APD array. Wire bonds were used to connect signals from the HgCdTe e-APD output at the fan-out contact pads on the substrate to the input of the ROIC. The substrate with the HgCdTe e-APD array and ROIC was mounted onto a leadless chip charier (LCC) to form a sensor chip assembly (SCA), as shown in Figure 2.

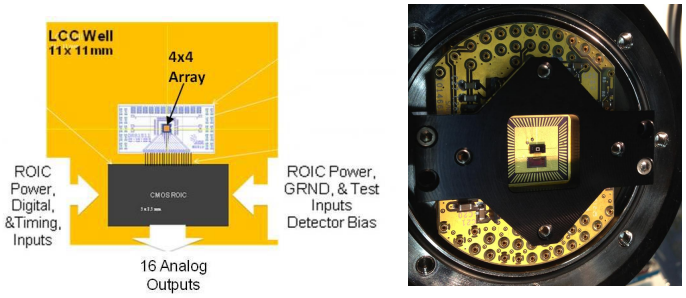

Figure 2. HgCdTe e-APD SCA, schematic (left) and photograph of the SCA inside the Dewar (right)

The SCA is housed in a closed-cycle Stirling cryocooler by SE-IR Corp. The support electronics including the APD bias control are integrated into a single circuit board with a field programmable gate array (FPGA) handling all the digital control signals. Figure 3 shows a photograph of the detector assembly. More details of the device can be found in Beck *et al*.[6] In this paper, we will describe the measurement results obtained at NASA Goddard Space Flight Center (GSFC).

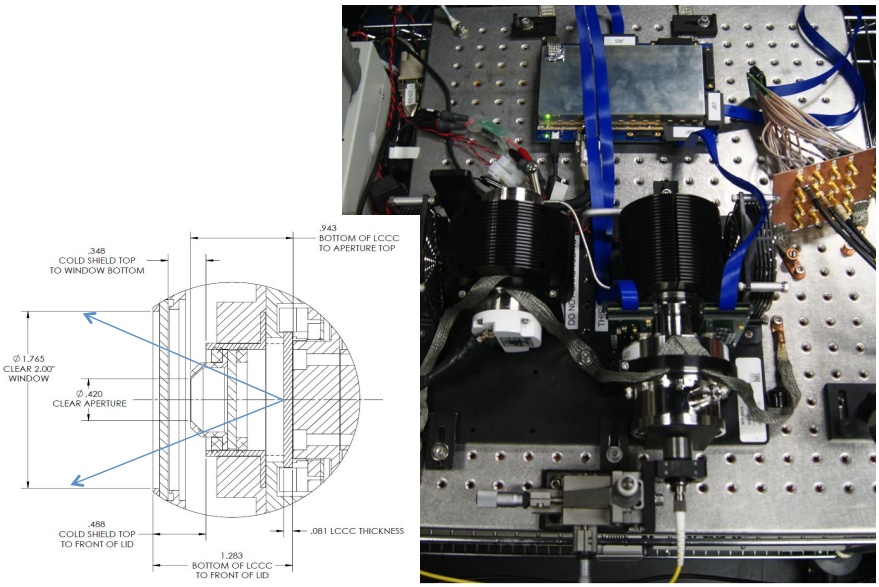

Figure 3. DRS 4x4 HgCdTe e-APD array detector assembly and the test setup at NASA GSFC.

2. TEST SETUP

The detector's response was first tested using a 1550 nm laser diode modulated by a external acousto-optics modulator to give 1 μs wide rectangular laser pulses. The laser light was attenuated and collimated onto the detector through the Dewar window and a cold filter. The HgCdTe e-APD array was flood illuminated during these tests. The amount of laser signal intercepted by each pixel was calibrated by measuring the laser pulse energy through a known size pinhole at the same distance as the SCA and scaling the results by the ratio of the pixel area to the pinhole area. A programmable attenuator was used to adjust the signal level. The signal level was also monitored with the use of an optical fiber splitter and a power meter. The outputs from the detector assembly were connected to an oscilloscope. A fast laser diode with 0.5 ns wide laser pulses was also used to measure the detector impulse response and later for linear mode photon counting tests. Figure 4 shows a block diagram of the entire test setup.

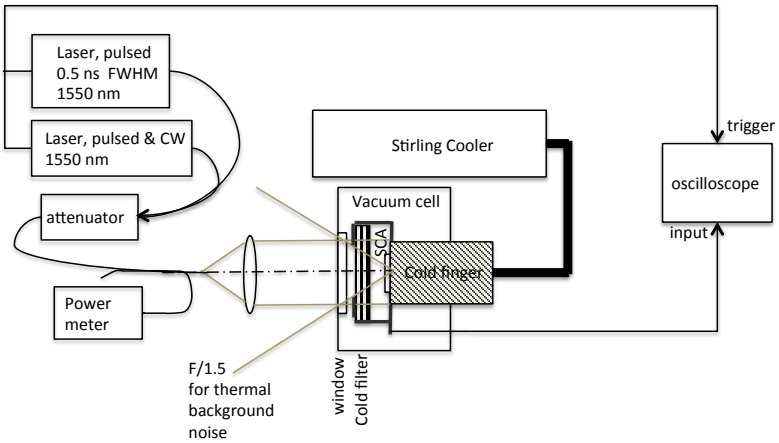

Figure 4. Test setup.

3. TEST RESULTS – PULSE DETECTIONS

The detector output in response to 1 μs wide rectangular pulses was measured at different input signal levels. Figure 5 shows sample pulse waveforms and the histograms of the signal and noise at an average signal of 100 photons/pulse net signal onto the detector surface along with the histograms of the pulse amplitude and baseline noise. The APD bias was set to 11 V APD bias (APD gain ~330) and the ROIC was set to the highest transimpedance gain. The pulse rise and fall time were about 50 ns after factoring out the contribution from the finite rise and fall times of the test source. Figure 6 shows the average pulse amplitude and the standard deviation (error bars) of the detector output as a function of the peak power of the incident optical signal at the same APD bias and ROIC gain setting.

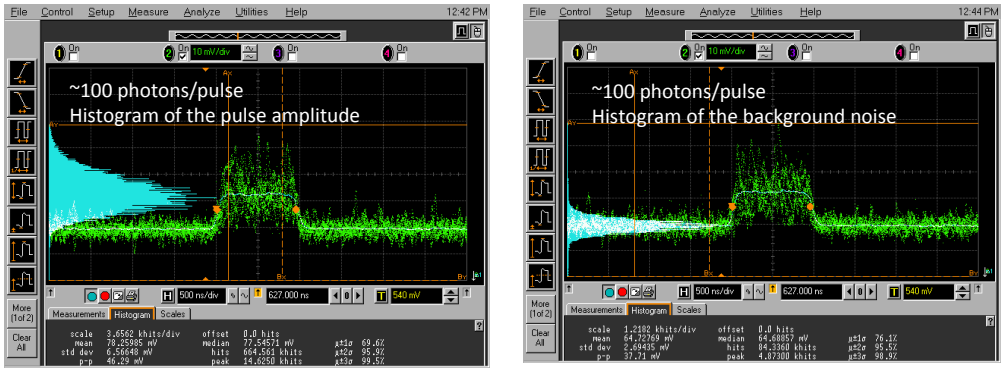

Figure 5. Sample detector output pulse waveforms and histogram of the pulse amplitude and baseline noise under about 100 photons per pulse net incident signal level. The APD bias was set to 11 V (APD gain ~330) and the ROIC was set to the highest transimpedance gain.

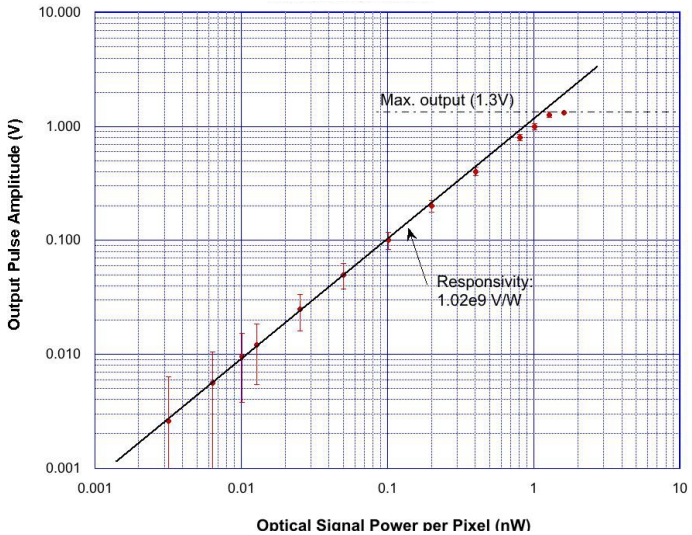

Figure 6. Mean and standard deviation (error bars) of the 4x4 HgCdTe e-APD array output as a function of the peak power of the net incident optical signal onto each pixel.

The detector responsivity in V/W and the baseline noise were measured as a function of the APD bias and the results are shown in Figure 7. The detector dark noise was measured at each APD bias voltage and it rose only slightly at the highest APD bias setting. The responsivity was the product of APD quantum efficiency, gain, fill-factor, ROIC gain, etc., which was measured individually at DRS during the component level testing before SCA integration.[6]

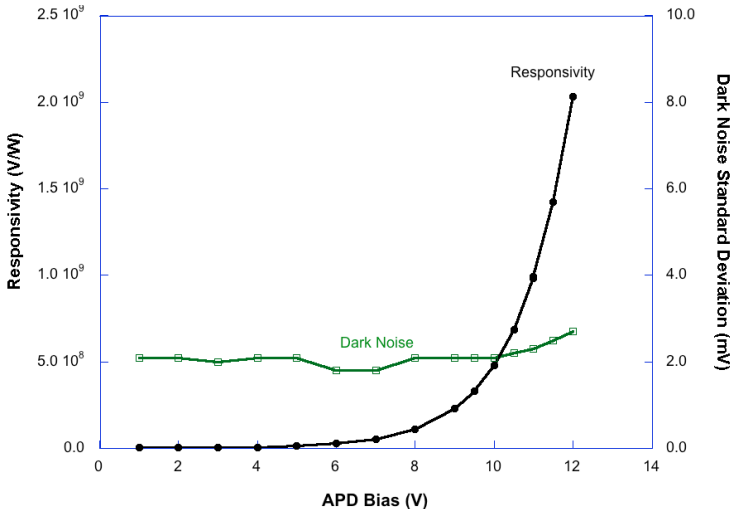

Figure 7. Detector responsivity and dark noise vs. the APD bias voltage.

The noise spectral density from the detector assembly was measured with a spectrum analyzer with the APD at zero bias (ROIC noise only) and 11.0 V APD bias with the device in dark and under a relatively strong continuous wave (CW) illumination, respectively. The result is shown in Figure 8. The total detector dark noise rose by about 2dB at 11 V APD bias, which indicated the APD dark noise started to override the ROIC noise at this APD gain. The noise spectrum under strong CW illumination gave a direct measurement of the detector electrical bandwidth, with a 3-dB bandwidth of about 6.2 MHz.

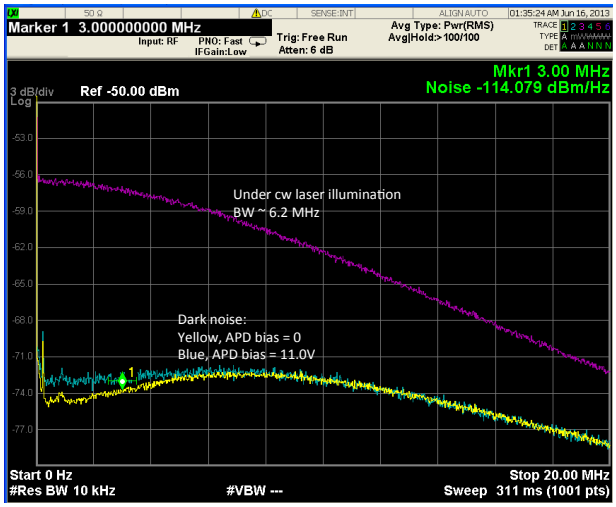

Figure 8. Noise spectral density at the output of the detector assembly at 0 and 11 V APD bias and dark and CW illumination, respectively.

The overall detector noise equivalent power (NEP) was obtained by dividing the standard deviation of the noise shown in Figure 7 by the responsivity of the detector and the square root of the bandwidth. They were 0.74 and 0.43 fW/Hz^{½} at 11 and 12 V APD bias, respectively. The NEP was also measured with the spectrum analyzer by first converting the noise spectral density in dBm/Hz to V/Hz^{½} by multiplying the 50-ohm load resistance of the spectrum analyzer and taking the square root, and then dividing the result by the detector responsivity. The two methods yielded approximately the same results.

The receiver signal to noise ratio (SNR), which was defined as the ratio of the mean to standard deviation of the output pulse amplitude, was measured as a function of the APD bias voltage for three incident signal levels, 100, 1000, and 6,300 average photons/pulse, as shown in Figure 9. The SNR first increased with the APD bias and hence the APD gain,

as the signal increased with APD gain to rise above the ROIC noise. As the APD bias increased the APD gain reached the point where the shot noise of the APD exceeded the ROIC noise. At this point the SNR becomes gain independent and starts to level off. At a certain APD bias, the SNR reached a plateau slightly below the quantum limits, which confirmed that the APD gain was noiseless and further increasing the APD gain had no adverse effect. The APD gain became sufficiently high at 11-12 V for incident signal levels from 100 to 1,000 photons/pulse, which is the typical signal level expected for the CO_2 lidar on the ASCENDS mission.

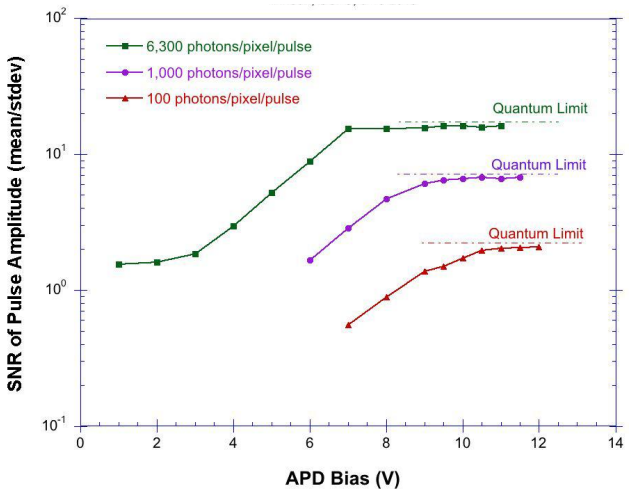

Figure 9. Receiver SNR as a function as the APD bias for incident signal levels of 100, 1000, and 6300 average number of photons per pulse per pixel in comparison to the quantum limits for ideal detectors. The measured SNR reached a plateau and stayed constant near the quantum limit, which showed that the APD gain was noiseless and the sufficient for signals above 100 photons/pulse.

The measurement results can be explained by the mathematical model of the APD, as

$$SNR \equiv \frac{mean}{stdev} = \frac{QE \cdot \langle G \rangle \frac{P_{peak}}{hf} q}{\sqrt{2q^2 F_{ex} \langle G \rangle^2 \frac{QE \cdot P_{peak}}{hf} BW_n + I_{circuit}^2 BW_n}} \tag{1}$$

where QE is the detector quantum efficiency, G is the APD gain, and P_{peak} is the peak optical signal power, q is the electrical charge, hf is the photon energy in Joule, $F_{ex} = \langle G^2 \rangle / \langle G \rangle^2$ is the excess noise factor of the APD gain, BW_n is the receiver noise bandwidth, and $I_{circuit}^2$ is the spectral density of the ROIC noise in A^2/Hz. The receiver noise bandwidth is assumed to be equal to 1.53 times the 3-dB signal bandwidth, like in a typical RC lowpass filter. As the APD gain increases, the contribution from the ROIC noise diminishes. For high APD gain,

$$SNR \to \frac{\sqrt{QE \frac{P_{peak}}{hf}}}{\sqrt{2F_{ex} BW_n}} = \frac{\sqrt{QE \langle n_{sig} \rangle}}{\sqrt{2F_{ex} BW_n \tau_{pw}}} = \sqrt{\frac{QE}{F_{ex}}} \times SNR_{QL} \tag{2}$$

where τ_{pw} is the laser pulse width, and $\langle n_{sig} \rangle$ is the average number of signal photons per pulse. The receive SNR approaches quantum limit and becomes independent of the APD bias only when the APD gain is 'noiseless' and the excess noise factor is approaching unity. Our measurements showed the SNR was about 0.9 times the quantum limit, therefore detector QE was about 80% for an excess noise factor of 1.0. Considering the fill factor, the actual APD quantum efficiency should be about 90%, similar to those measured at DRS.[6]

4. TEST RESULTS – LINEAR MODE PHOTON COUNTING

The high APD gain, low dark noise and low ROIC noise enabled using these 4x4 HgCdTe e-APD arrays for linear mode photon counting, even though the devices were not optimized for detecting single photon events. The photon counting efficiency (PDE) and the maximum count rate would be much improved with a higher bandwidth ROIC while maintaining similar NEP. DRS is currently developing a higher bandwidth HgCdTe e-APD ROIC assembly under an Advanced Component Technology (ACT) program from NASA ESTO.[7,8] The new detector is expected to have a much better performance in linear mode photon counting operation. The measurements with the 4x4 HgCdTe e-APD detector showed the ultimate sensitivity of the current 4x4 HgCdTe e-APD array and gave a preview of the new devices.

The receiver impulse response was measured by illuminating the detector with the narrow pulse width (0.5 ns) laser and the result is shown in Figure 10. The full width at half maximum (FWHM) of the detector output pulse width was 60-70 ns. To optimized the SNR for single photon pulses, a 9-pole Bessel lowpass filter was added at the output of the detector. The lowpass filter had a 3-dB bandwidth of 8.3 MHz and a near Gaussian impulse response with about 60 ns FWHM.

Figure 10. Impulse response of the HgCdTe e-APD output. It was measured as the detector output pulse waveform in response to a 0.5 ns FWHM laser pulses. The impulse pulse width was 60-70 ns FWHM with a rise and fall times of about 50 ns.

To measure the photon counting performance, a discriminator and a multi-channel scaler was used besides the oscilloscope to produce histogram of the detected photons over consecutive time bins. The discriminator threshold level was first varied over a wide range while monitoring the detector dark and the photon count rates at a given CW illumination. The results are shown in Figure 11. The optimal threshold was chosen which give the highest net photon count rate.

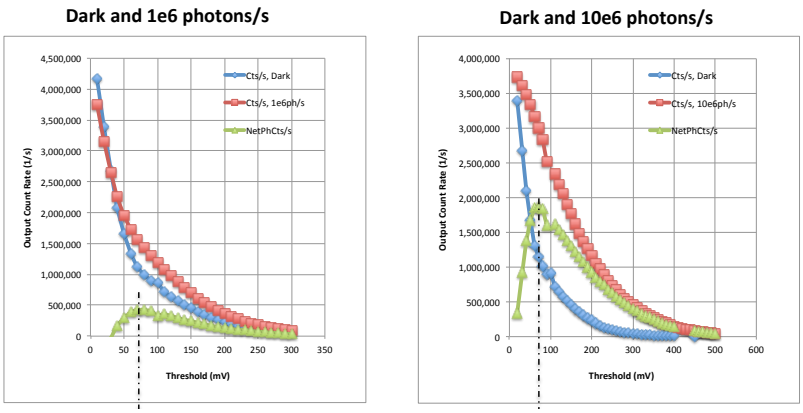

Figure 11. Detector output count rates vs. discriminator threshold levels under dark and 1e6/s and 10e6/s incident photons/s per pixel. The optimal threshold for photon counting was found to be 70 mV.

The count rate of the detector output at the optimal discriminator threshold was measured by the frequency counter as a function of incident photon rate. Figure 12 shows the measured count rate as a function of the incident photon rate. The detector dark count rate was about 1.2 Mcts/s, which was mostly due to the residual background photons in the Dewar. It shows the PDE of this detector was about 37% even though the detector was not optimized for photon counting. The maximum count rate was limited to 3-4 Mcts/s mostly due to the limited electrical bandwidth of the ROIC.

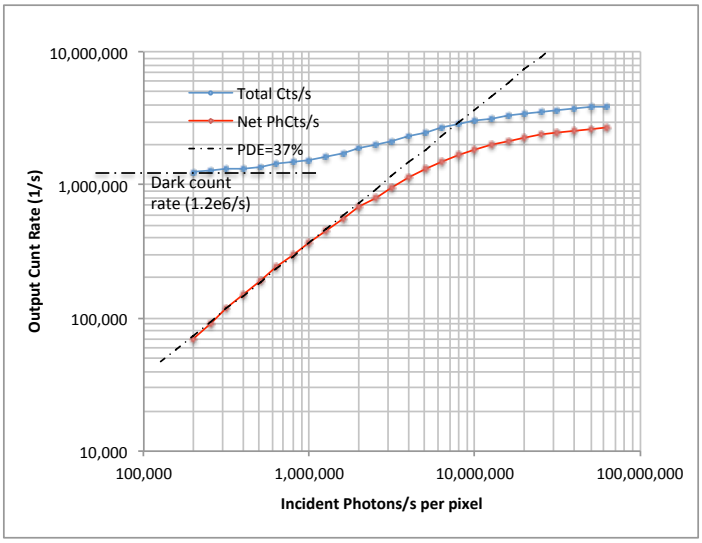

Figure 12. Detector output count rates from one of the pixel as a function of the incident photons/s. The discriminator threshold was set to 70 mV, the optimal value according to Figure 11.

Figure 13 shows the distribution of the dark counts and the total counts under 10e6/s incident photons measured by the multi-channel scaler at about 100 mV threshold level.

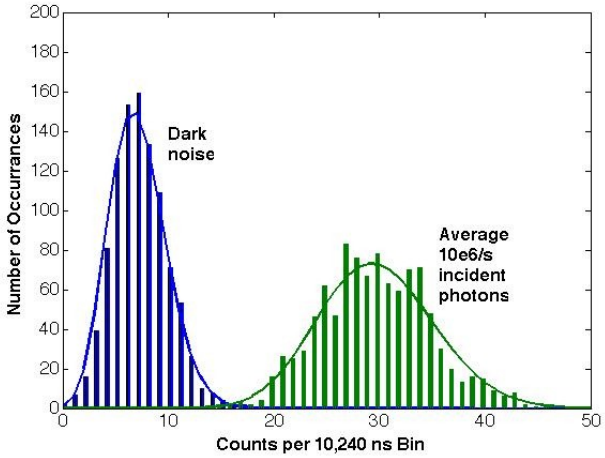

Figure 13. Distribution of the counts from one of the pixel per 10,240-ns bin under dark (blue) and 10 Mcts/s incident photons (green). The solid curves are the Poisson distribution functions of the same average values of the counts per bin in dark and under illumination.

Auto-correlation function of the detected photon and dark counts was calculated and it remained zero except at zero time shift, as in an ideal Poisson distributed photon counting process. There was no afterpulsing or other nonlinear effects.

We also directly measure the afterpulsing by illuminating the detector with short laser pulses and looked for tails in the histogram immediately after the pulse detection. There was no measureable afterpulsing.

Lastly, we measured the detector output pulse waveform in response a 0.5 ns wide laser pulse at different incident signal level. Because of the relative short laser pulse width, all photons could be assumed to arrive at the same time. Figure 14 shows sample pulse waveforms and histogram of the pulse amplitude under different incident signal level. Figure 15 shows the output pulse amplitude and standard deviation as a function of the incident photons/pulse per pixel.

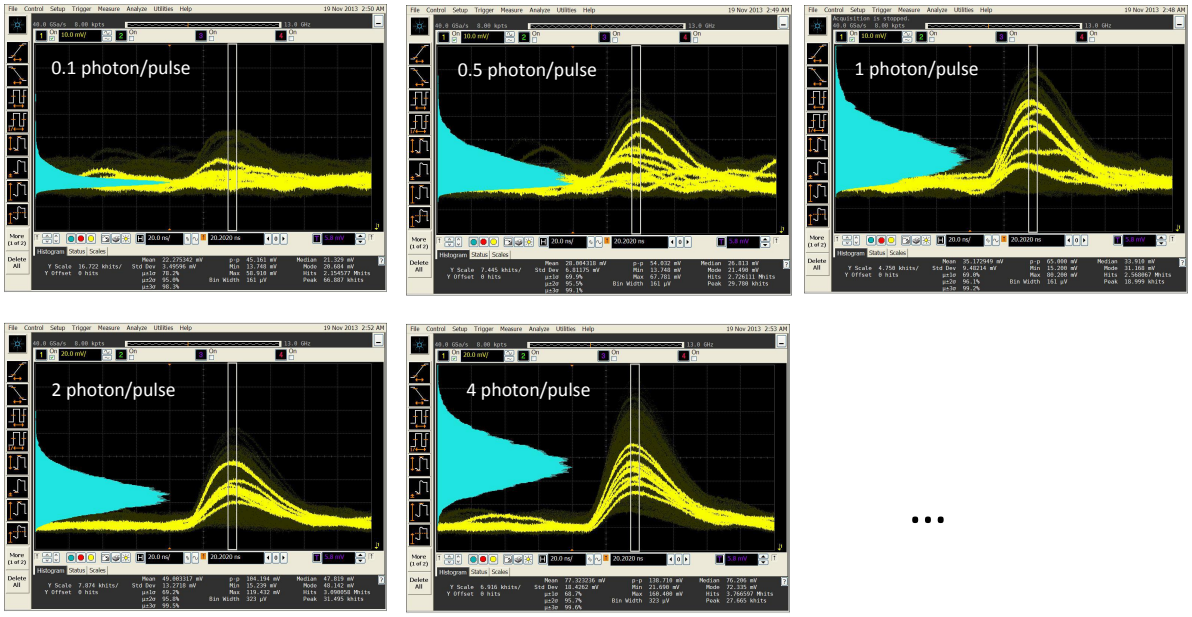

Figure 14. Pulse waveforms and histogram of the pulse amplitude measured at the peak of the pulses from one of the 16 pixels of the 4x4 HgCdTe e-APD array in response to 0.5 ns wide laser pulses at different incident signal levels.

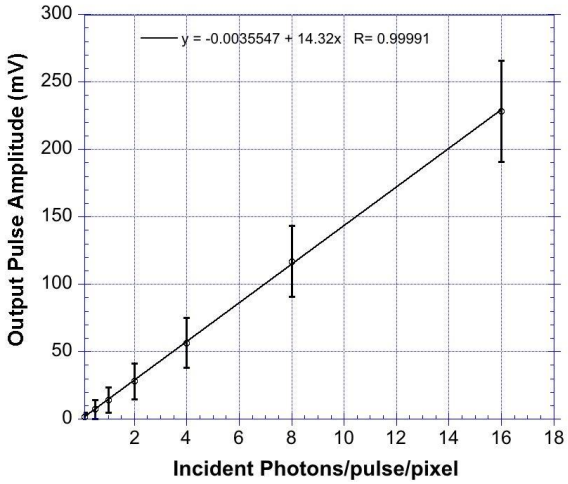

Figure 15. Average pulse amplitude and standard deviation from one of the 16 pixels of the 4x4 HgCdTe e-APD array in response to 0.5 ns wide laser pulses and different incident signal level.

5. CONCLUSIONS

DRS Technologies has developed an HgCdTe electron initiated avalanche photodiode (e-APD) focal plane array as a candidate lidar detector for NASA's Active Sensing of CO_2 Emission over Days, Nights, and Seasons (ASCENDS) mission. The detector had 80-μm pixels arranged in a 4x4 array. As part of this work, a custom 16-channel read-out integrated circuit (ROIC) was developed and integrated with the HgCdTe e-APD array. The detector and ROIC operated at 77K inside a small closed-cycle Dewar with the APD bias circuit and other support electronics integrated in a field programmable gate array (FPGA). The tests at NASA Goddard Space Flight Center showed the device had about 90% quantum efficiency at 1.55 μm and a noise equivalent power (NEP) of <0.5 fW/Hz$^{1/2}$ at an APD bias of 12 V. The electrical bandwidth was 6.2 MHz, selected to match the CO_2 lidar laser pulse shape. The test results also showed no measurable excess noise and sufficiently high APD gain to override the ROIC noise and achieve near quantum-limited performance for the CO_2 lidar. The high APD gain, low dark noise, and low ROIC noise also enabled the device to be used for linear mode photon counting (LMPC) operation despite of the 6.2 MHz ROIC electrical bandwidth. Ongoing work is integrating this detector into NASA Goddard's CO2 lidar and plans are to demonstrate its performance in airborne measurements during the summer of 2014. A new series of LMPC HgCdTe e-APD arrays with a much high ROIC bandwidth are currently being developed at DRS with support from NASA Earth Science Technology Office (ESTO). These HgCdTe e-APD detectors fill a gap in single photon detectors for wavelengths between 0.9 to 4.3 μm and will enhance the performance of space lidar and other remote sensing instruments.

6. ACKNOWLEDGEMENTS

This work was supported by the NASA ESTO IIP program that is managed by Parminder Ghuman and Irene Bibyk.

REFERENCES

[1] Abshire, J. B., Ramanathan, A., Riris, H., Mao, J., Allan, G. R., Hasselbrack, W. E., Weaver, C. J., and Browell, E. V., "Airborne measurements of CO_2 column concentration and range using a pulsed direct-detection IPDA lidar," Remote Sensing 6, 443-469 (2014).

[2] Riris, H., Numata, K., Li, S., Wu, S., Ramanathan, A., Dawsey, M., Mao, J., Kawa, R. and Abshire, J. B., "Airborne measurements of atmospheric methane column abundance using a pulsed integrated-path differential absorption lidar," Applied Optics 51(34), 8296-8305 (2012).

[3] Beck, J., Wan, C., Kinch, M., Robinson, J., Mitra, P., Scritchfield, R., Ma, F., and Campbell, J., "The HgCdTe Electron Avalanche Photodiode," IEEE LEOS Newslett. 20(5), 8-12 (2006).

[4] Kinch, A. M., [Infrared Detector Materials], SPIE Press, Bellingham (2007).

[5] Raab, J., and Tward, E., "Northrop Grumman Aerospace Systems cryocooler overview," Cryogenics 50(9), 572-581 (2010).

[6] Beck, J., McCurdy, J., Skokan, M., Kamilar, C., Scritchfield, R., Welch, T., Mitra, P., Sun, X., Abshire, J., and Reiff, K., "A highly sensitive multi-element HgCdTe e-APD detector for IPDA lidar application," Proc. SPIE 8739, 83790V (2013).

[7] Beck, J. D., Scritchfield, R., Mitra, P., Sullivan, III, W. W., Gleckier, A. D., Strittmater, R., and Martin, R. J., "Linear mode photon counting with the noiseless gain HgCdTe e-avalanche photodiode," Optical Engineering 53(8), 081905 1-10 (2014).

[8] Beck, J. D., Kinch, M., and Sun, X., "Update on linear mode photon counting with the HgCdTe e-APD," Optical Engineering 53(8), 081906 1-8 (2014).